Flexible and conductive *meta*-aramid fiber paper with high thermal and chemical stability for electromagnetic interference shielding

Yanfen Zhou[†, ‡, ¶], Zhenhua Sun[†, ¶], Liang Jiang[†, *], Shaojuan Chen[†, ǁ], Jianwei Ma[†, ‡, *], Fenglei Zhou[†, §]

[†]College of Textiles and Clothing, Qingdao University, Qingdao, 266071, P. R. China

[‡]Industrial Research Institute of Nonwovens and Technical Textiles, Qingdao, 266071, P. R. China

[ǁ]Eco-Textile Collaborative Innovation Center, Qingdao University, Qingdao, 266071, P. R. China

[§]Centre for Medical Image Computing, University College London, London, WC1V 6LJ, UK

*Corresponding authors: mjwfz@qdu.edu.cn (Jianwei Ma), liang.jiang@qdu.edu.cn (Liang Jiang)

[¶] Yanfen Zhou and Zhenhua Sun contributed equally to this work.

ABSTRACT: How to function properly under extreme working conditions is a key challenge for flexible electronic devices because their performance is often susceptible to environmental conditions. Herein, we demonstrated the fabrication, evaluation, and application of a flexible and highly conductive *meta*-aramid fiber paper (MAFP) by combining oxygen plasma treatment and electroless silver plating. The plasma treatment etched the MAFP surface and introduced large amounts of oxygen-containing groups which led to the formation of continuous silver coating and high interface binding between MAFP and Ag nanoparticles. The results showed that the silver-coated MAFP had an electrical resistance as low as 0.152 Ω/sq and exhibited excellent temperature, mechanical and chemical stability. Finally, these properties of silver-coated MAFP were exploited for its use as electromagnetic interference (EMI) shielding. Experimental results revealed that the EMI shielding effectiveness (SE) of the silver-coated MAFP reached as high as 95.47 dB and a specific EMI SE of 530.38 $dB \cdot mm^{-1}$. These results have clearly demonstrated that MAFP can become highly electrically conductive after simple plasma treatment and silver coating while keeping its excellent thermal and chemical stability and therefore holds great promise for the development of new kinds of all-weather flexible electronic devices.

KEYWORDS: *meta*-aramid fiber paper; plasma treatment; silver nanoparticles; electrical conductivity; electromagnetic interference shielding

1. Introduction

Traditional silicon or indium tin oxide-based electronic components which are rigid and brittle cannot meet the requirements for flexible devices that can function under extreme environments [1]. Due to increasing demands for flexible, lightweight, and portable electronic devices, flexible electronic devices have been developed for applications in

various fields including wearable devices [2] and electromagnetic shielding [3]. However, flexible electronic devices are still subject to the susceptibility to the extreme conditions. For example, the exposure to oxidation and corrosion of metal-based conductive materials could degrade their performance inevitably and even lead to a failure in function over time [4]. Moreover, moisture, icing, and snowing could deteriorate the performance of flexible electronic devices [5]. The capability of flexible electronic devices to exhibit stable performance in the flame is also particularly important for applications in fire disasters [6]. As a consequence, there is a strong interest in high performance flexible conductive materials. *Meta*-aramid fiber paper (MAFP) is a kind of high-performance paper made by hot pressing of *meta*-aramid staple and pulp fibers. Featured with good thermal stability, excellent mechanical properties and easy deformation [7, 8], MAFP is potentially a good candidate for preparing flexible conductive materials.

Flexible conductive materials can be made by filling conductive fillers into polymer matrix [9,10] or coating conductive components onto the surface of existing polymeric substrates [11, 12]. Carbon nanotubes (CNTs) [13-16], graphene [17-19], metal nanowires and nanoparticles [20-22] are considered as ideal conductive components owing to their high conductivity and excellent mechanical robustness. Compared with other conductive components, silver has the highest conductivity (1.65×10^{-8} Ω·m of resistivity) [23] and hence is considered to be the best candidate for fabricating conductive composite materials. Generally used methods to prepare silver nanoparticle functionalized materials include electroless plating, electroplating, sputtering method and self-assembly [24-26]. Among these methods, electroless plating is the most widely used one due to simple operation, uniform coating and low cost [27-29]. However, as the surface chemical energy of *meta*-

aramid fibers is very low and the reaction activity is very weak [30, 31], direct electroless plating of silver nanoparticles on *meta*-aramid is very difficult. Therefore, an effective surface modification of *meta*-aramid fibers is required before electroless plating.

Plasma treatment has the advantages of convenience and environmental friendliness and more importantly, it has the capacity to activate the surface of substrates [32]. During plasma processing, many electrons, ions and metastable ions in the ion flow can break the molecular chain on the surface in a short time, increase the number of active groups and unsaturated bonds, and meanwhile play a certain etching effect [33-35]. Plasma treatment occurred only on the surface without affecting the elemental composition and macroscopic mechanical properties of the substrate [36, 37]. Therefore, low-temperature oxygen plasma treatment could be employed to treat MAPF before silver plating.

In this work, commercially available *meta*-aramid fiber paper was made highly conductive by combining low-temperature oxygen plasma treatment and electroless silver plating. The resultant MAFP showed sheet resistance as low as 0.152 Ω/sq. Also, the electrical conductivity of silver-coated MAFP remained still very satisfying after being washed and bended for many times. More importantly, the silver-coated MAFP exhibited good stability in a wide range of temperature of -80 °C to 200 °C and resistance to acid/alkali solutions and various organic harsh solvents. Finally, the potential application of silver-coated MAFP was demonstrated in the area of electromagnetic interference (EMI) shielding, showing high EMI shielding efficiency.

2. Experimental

2.1. Materials and chemicals

The *meta*-aramid fiber paper (MAFP) with a thickness of 0.18 mm and a fiber diameter of 21.5 μm was supplied by ZhongFang Special Fiber Co., Ltd, Dongying, China. Silver nitrate ($AgNO_3$), Glucose, Sodium hydroxide (NaOH), hydrochloric acid (HCl), ammonia ($NH_3 \cdot H_2O$), ethanol, acetone, N, N-dimethylformamide (DMF), N-heptane and xylene were purchased from Sinopharm Chemical Reagent Co., Ltd, China. All the chemicals were used as received without any further treatment.

2.2. Preparation of silver-coated MAFP

Firstly, the MAFP was washed with a 50% ethanol solution to remove surface impurities and dried. Then, the MAFP was treated by using a plasmatreater (AS 400, Plasmatreat GmbH, Germany). The power of the plasmatreater was 6000 W. The MAFP was treated at the nozzle speed of 1 m/min, plasma cycle time of 80% and nozzle height of 4 cm. For a MAFP sample with a size of 5 × 5 cm^2, the plasma processing time for a single side was about 1 min. In order to ensure the timeliness of plasma treatment [38, 39], the plasma-treated MAFP was immersed immediately in the pre-prepared ammoniacal silver nitrate solution (with a concentration of 20 g/L) which was used for the subsequent deposition of silver nanoparticles. After soaking for 30 min, glucose solution with a concentration of 30 g/L was added to the above mentioned ammoniacal silver nitrate solution with a rate of about 60 drops/min and magnetically stirred. The electroless plating process was allowed to proceed at room temperature for 24 hours. Finally, the silver-coated MAFP was rinsed with deionized water three times and dried in vacuum oven at 60 °C for 24 hours.

2.3. Characterization and measurement

The surface morphology of MAFP was observed by using scanning electron microscopy (SEM) (VEGA3, TESCAN, Czech), which is equipped with an energy dispersive

spectrometer (EDS). The SEM images were taken at a voltage of 10 kV. Three-dimensional surface morphology of MAFP was observed by using atomic force microscopy (AFM, CSPM5500, Beijing Nano-Instruments, China). The chemical bond and elemental composition of MAFP surface were determined by using an X-ray photoelectron spectroscopy (XPS) (ESCALAB 250XI, Thermo Fisher Scientific, USA) with an Al Kα X-ray source (1486.6 eV photons). All binding energies (BEs) referenced to the C1s hydrocarbon peak at 284.6 eV to compensate for surface charging effects. The water contact angle was tested by using an automatic contact angle measuring instrument (XG-CAMD3, Shanghai Xuanyichuangxi Industrial Equipment Co., Ltd. China). The measurement was conducted by using the static drop method (the amount of liquid added was 10 ± 0.1 μl and the measuring resolution was 0.01°). The X-ray diffraction pattern was obtained by exploiting an X-ray diffractometer (XRD) (Rigaku Ultima IV, Japan) using Cu Kα radiation with a wavelength of 1.54056 Å, the patterns were recorded in the 2θ range from 5 to 90° with a scanning speed of 5°/min and a step of 0.02°. Thermal property of MAFP, plasma-treated MAFP and silver-coated MAFP was studied by using a TG/DSC Synchronous thermal analyzer (STA 449 F3, NETZSCH GmbH, Germany). The thermal decomposition curves were recorded in the temperature range of 40 – 800 °C with a heating rate of 20 °C/min. The content of silver (w_{Ag}) was calculated from TG data according to the following equation:

$$w_{Ag} = \frac{w_a - w_b}{1 - w_b} \quad (1)$$

Where w_a and w_b is the residual mass fraction of silver-coated MAFP and pristine MAFP respectively. The sheet resistance of silver-coated MAFP was measured by using a multifunction digital four-probe tester (ST-2258C, Suzhou Jingge Electronic Co., Ltd, China)

under standard atmospheric condition (20 °C/65% RH). The EMI shielding effectiveness of the silver-coated MAFP was investigated by using an ENA network analyzer (ZNB 20, Rohde & Schwarz, Germany) in the frequency range of 8.2 – 12.4 GHz (X band) by means of waveguide method at room temperature.

3. Results and discussion

3.1. Effect of plasma treatment on electroless deposition of Ag on MAFP

Fig. 1 illustrates the process of preparing silver-coated MAFP. Briefly, the MAFP was treated with oxygen plasma to active the surface and then functionalized with silver nanoparticles through the electroless plating method. Microstructure observation shows that the surface of pristine MAFP had obvious gully region (Fig. 2a), which was caused by the interweaving and bonding of *meta*-aramid pulp and staple fibers. After oxygen plasma treatment, the surface of MAFP was etched, resulting in ripple-like texture and multiple etching spots on staple fibers (Fig. 2b). Three-dimensional surface topography shows that the surface of MAFP became rougher after plasma treatment (Fig. 2c and d).

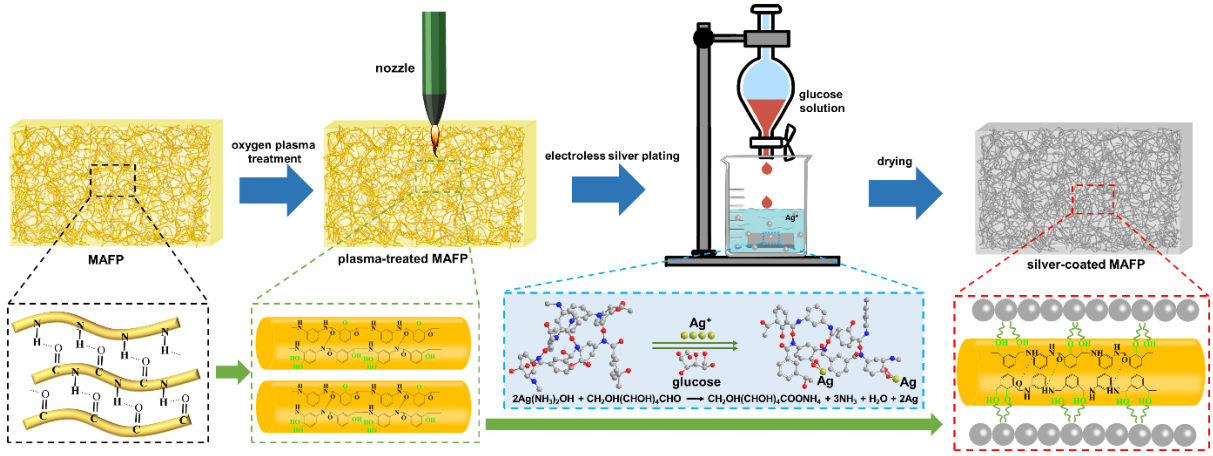

Fig. 1. Schematic illustration of the procedure for preparing silver-coated MAFP with plasma treatment.

The plasma treatment also induced significant changes in surface chemical composition of MAFP. The results of XPS wide-scan (Fig. 2e and Table 1) show that the carbon content, O/C ratio and N/C ratio of pristine MAFP was 85.22%, 0.14 and 0.03 respectively, whereas in contrast, the carbon content of plasma-treated MAFP decreased to 46.19% while the oxygen content increased from 12.25% to 49.09%. In particular, the O/C ratio raised significantly from 0.14 to 1.06 after plasma treatment. The C 1s core-level spectrum of the pristine MAFP can be curve fitted with three peak components having binding energies (BEs) of 284.5 eV for the -C-C-/-C-H species, 285.5 eV for the -C-N- species and 287.8 eV for the -C=O species (Fig. 2f). These peaks are attributed to the benzene ring and amide bonds present in *meta*-aramid molecule. Two additional peak components at 286 eV and 288.9 eV, which are ascribed to -C-O- and -COO- [32], appeared on the plasma-treated MAFP (Fig. 2g). The content of -C-C-/-C-H, -C-N- and -C=O in pristine MAFP was 90.13%, 4.70% and 5.18% respectively. However, for plasma-treated MAFP, the content of -C-C-/-C-H decreased obviously to 78.03%, while new oxygen-containing groups including -C-O- and -COO- were formed, with the content of 2.38% and 3.41% respectively. These results suggest that oxygen plasma treatment increased both the type and the amount of active oxygen-containing groups on the MAFP surface. As shown in Fig. 2h and 2i, the static water contact angle of MAFP decreased from 101.8° to 55.8° after plasma treatment, indicating a clear increase in wettability.

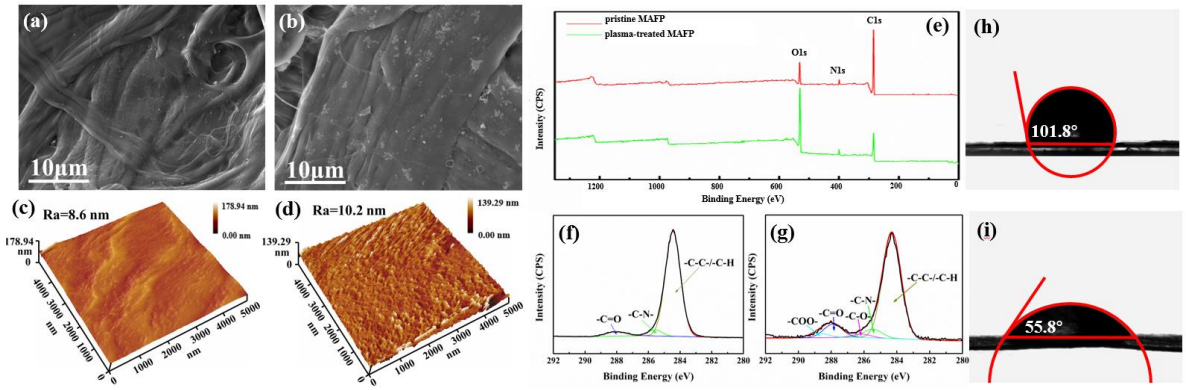

Fig. 2. SEM and AFM images of pristine MAFP (a and c), plasma-treated MAFP (b and d); XPS wide-scan spectra of pristine MAFP and plasma-treated MAFP (e); XPS spectra of C 1s peaks for pristine MAFP (f) and plasma-treated MAFP (g); the water contact angle of pristine MAFP (h) and plasma-treated MAFP (i).

Table 1. Chemical compositions and the content of functional groups on the surface of pristine MAFP and plasma-treated MAFP.

Sample	Chemical composition (at.%)			Atom ratio		Content of functional group (%)				
	C 1s	O 1s	N 1s	O/C	N/C	-C-C-/ -C-H	-C-N-	-C-O-	-C=O	-COO-
Pristine MAFP	85.22	12.25	2.52	0.14	0.03	90.13	4.70	0	5.18	0
Plasma-treated MAFP	46.19	49.09	4.72	1.06	0.10	78.03	6.37	2.38	9.81	3.41

As can be seen from Fig. 3a, the obtained silver-coated MAFP could be bent without breaking, showing high flexibility. A compact and uniform silver coating can be observed clearly on the MAFP surface (Fig. 3b). The coating thickness was approximated to be about 270 nm (Fig. S1, Supplementary data). The formation of continuous silver coating layer was because the introduction of electronegative oxygen groups after plasma treatment greatly improved the surface wettability of MAFP, which could effectively facilitate the absorption of silver ions and the subsequent deposition of silver nanoparticles. In addition, as these oxygen-containing polar functional groups could form ionic and covalent interacting with Ag nanoparticles, the interface binding between MAFP and Ag nanoparticles would be greatly strengthened [40].Three-dimensional surface morphology observation shows that the surface roughness of silver-coated MAFP (Fig. 3c) was larger than that of the pristine and plasma treated MAFP (Fig. 2c and 2d). XRD patterns in Fig. 3d show that the pristine MAFP had diffraction peaks at 2θ values of 23.4° and 27.0°, indicating that it was partially crystallized [28]. The MAFP before and after plasma treatment had the same diffraction peaks as pristine MAFP, suggesting that plasma treatment had no effect on the crystal structure of MAFP. New characteristic peaks at 2θ values of 38.2°, 44.4°, 64.5°, 77.5°, 81.6°, which corresponds respectively to the (1 1 1), (2 0 0), (2 2 0), (3 1 1) and (2 2 2) planes of face-centered cubic lattice (FCC) phase silver (JCPDS card No. 04-0783) [28] present in the XRD pattern of silver-coated MAFP. This confirms the successful deposition of silver nanoparticles on the MAFP surface. No other diffraction peaks were observed, indicating that the coated silver was in elemental form.

Thermal decomposition curve was used to demonstrate the thermal stability of MAFP and to quantify the content of silver coating in silver-coated MAFP. It can be seen from Fig. 3e that

the weight loss of pristine MAFP was a two-stage process. For the 1st stage, a small weight loss of about 3.16% occurred between 40 and 200 °C, which was caused by the evaporation of bound water and residual solvent contained in the material. For the 2nd stage, the initial thermal decomposition took place at 430 °C, indicating the high thermal stability of MAFP. A distinct weight loss of 41.55% between 400 and 800 °C was attributed to partial dehydroxylation and alkoxide decomposition in the material. The silver-coated MAFP showed a similar first stage as pristine MAFP, with a weight loss of 2.24% up to 200 °C. The sample began to decompose at around 430 °C and had a weight loss of 36.76% at 800 °C. According to Eqn.1, the silver content of silver-coated MAFP was 12.72%.

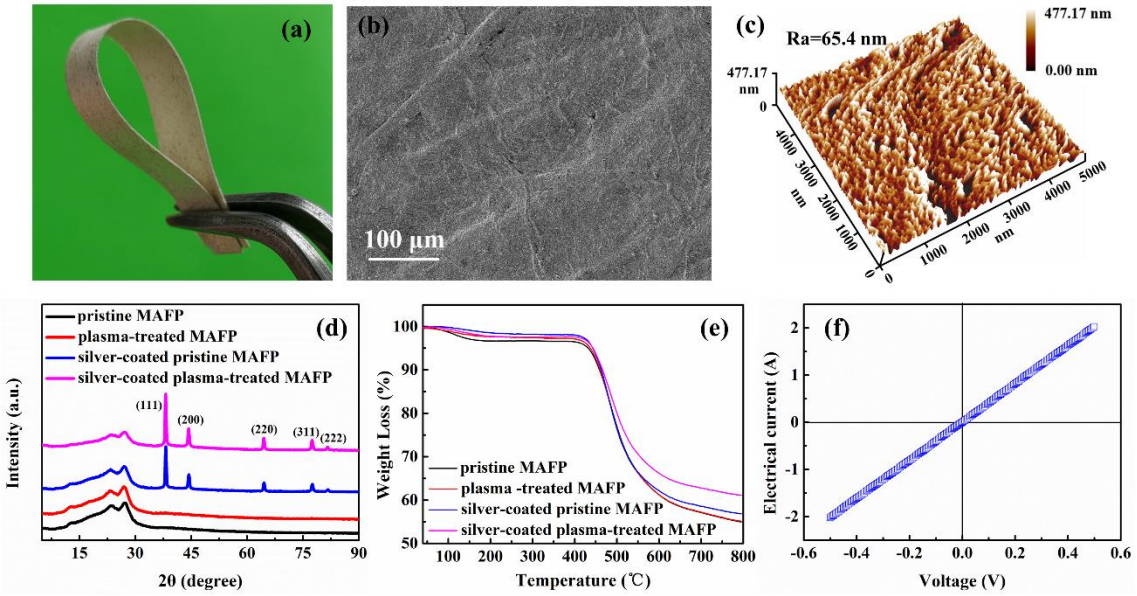

Fig. 3. The bending demonstration (a), SEM image (b) and AFM image (c) of silver-coated MAFP with plasma treatment; the XRD patterns (d) and TG curves of different MAFP (e); the volt-ampere characteristic curve of silver-coated MAFP with plasma treatment (f).

The electrical sheet resistance of silver-coated MAFP reached 0.152 Ω/sq, which was lower than similar materials in respect of electrical conductivity [41-47]. The volt-ampere characteristics of the obtained silver-coated MAFP with plasma treatment was found to adhere to Ohs' law (Fig. 3f).

In order to demonstrate the effect of plasma treatment on the deposition of silver nanoparticles on MAFP surface, silver-coated MAFP without plasma treatment was prepared as control. The XRD patterns in Fig. 3d show that silver element was also present in silver-coated MAFP without plasma treatment and the silver content was 4.13% as indicated by the TG measurement (Fig. 3e), but the sample showed no electrical conductivity because continuous silver coating was not formed as can be seen from the SEM observation (Fig. S2, Supplementary data). This confirms the beneficial effect of plasma treatment.

3.2. Washing and bending fastness of silver-coated MAFP

Flexible conductive materials should exhibit satisfactory performance stability under washing and mechanical deformation to satisfy their practical applications. The washing and bending stability of silver-coated MAFP was evaluated. The washing stability was conducted by subjecting the silver-coated MAFP in water bath with a constant temperature at 40 °C for 5 cycles (30 min/cycle) by using a textile-color fastness meter (SW-20B, Quanzhou MeiBang Instrument Co., Ltd, China) (the inserted image in Fig. 4a). The bending stability was evaluated by subjecting the samples to 1000 bending cycles at a constant bending strain of 50% (the inserted image in Fig. 4b). It can be seen from Fig. 4a and 4b that the sheet resistance of silver-coated MAFP increased from 0.198 to 0.406 Ω/sq after 5 washing cycles and increased from 0.182 to 0.329 Ω/sq after 1000 bending cycles. The increase in electrical resistance after washing and bending was due to the small amount peeling-off of the silver

coating and the generation of tiny cracks on the coating layer, respectively (Fig. 4c and e). However, most of the coating layer remained good after washing and bending tests (Fig. 4d and f), which contributed to the maintenance of high electrical conductivity after washing and bending. This was further confirmed by connecting the sample with a commercial light bulb (3.8 V/0.3 A) under an applied voltage of 3 V, as illustrated in Fig. 4g. It can be seen that the electrical current of the circuit with only the bulb was 0.288 A. When the silver-coated MAFP was inserted in the circuit and formed a current loop, the bulb was lighted well and the electrical current was 0.286 A. When the silver-coated MAFP after 5 washing cycles or 1000 bending cycles was connected in the circuit, the electrical current decreased slightly to 0.281 A and 0.280 A respectively. This verifies the excellent electrical conductivity and good stability under washing and bending of the silver-coated MAFP.

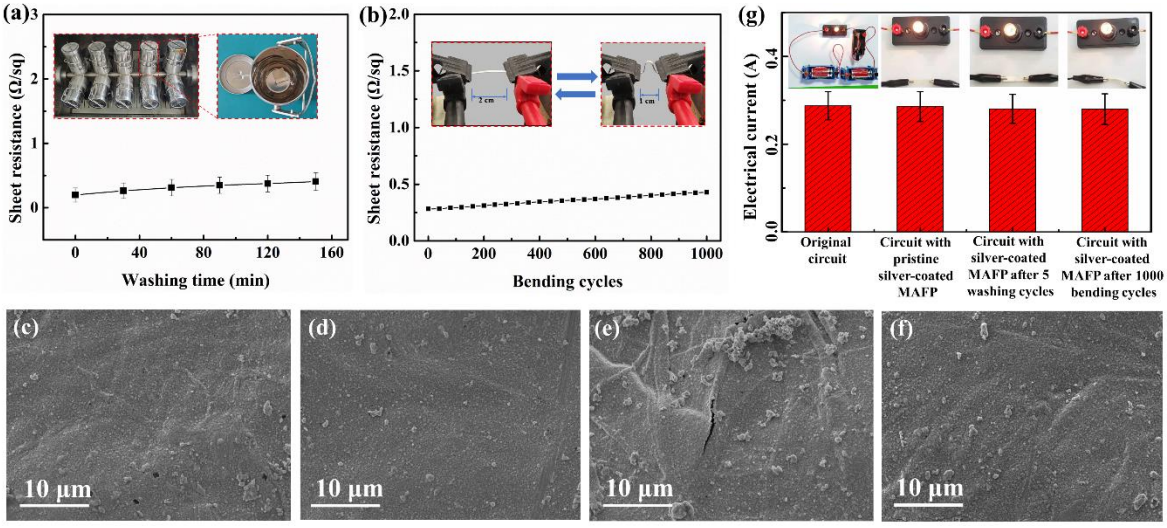

Fig. 4. The variation of sheet resistance of silver-coated MAFP with washing cycles (a); the variation of sheet resistance of silver-coated MAFP with bending cycles (b); SEM images of silver-coated MAFP after 5 washing cycles (c, d) and 1000 bending cycles (e, f); the electrical

current of the circuit without and with silver-coated MAFP under a direct current power supply at a voltage of 3 V (g).

3.3. Performance evaluation under extreme condition

The increasing use of flexible electrically conductive materials in various fields highlights their susceptibility to various environmental conditions. In this section, the electrical conductivity stability of the silver coated MAFP under various extreme conditions including high/low temperature, acid/alkali solutions and various organic solvents was evaluated.

In order to test the conductivity of silver-coated MAFP at extreme temperature, silver-coated MAFP was first placed in oven (air atmosphere) or ultra-low temperature freezer for 2 h and then the sheet resistance of the sample was measured. Fig. 5a shows the variation of electrical resistance of silver-coated MAFP after being subjected to different temperature for 2 h. It can be seen that the sheet resistance of silver-coated MAFP varied little between 0.105 Ω/sq and 0.183 Ω/sq in the temperature range of -80 °C – 200 °C, indicating good temperature stability.

The electrical conductivity stability of silver-coated MAFP was further demonstrated by exposing the sample to ice. Fig. 5b shows the variation of the electrical current through the silver-coated MAFP connected with a direct current power supply at 3 V (B2901A, Keysight, USA) and a bulb during the exposure process of the paper to ice. We can see that the electrical current was almost unchanged when the silver-coated MAFP was in direct contact with ice for 60 min when the ice didn't totally melt. The brightness of the bulb connected with the silver-coated MAFP also remained nearly unchanged during the test (Fig. 5d). This indicates the potential application of the prepared silver-coated MAFP in wet and cold conditions.

An increasing number of electric fire accidents underline the importance of flame-retardance of flexible conductive materials [48]. In this work, we investigated the flame retardancy of the silver-coated MAFP. The experimental setup for the flame-retardant tests was designed on the basis of the vertical combustibility method, as schematically shown in the inserted image of Fig. 5c. For comparison, conventional cellulose paper having the same dimensions as the MAFP was used as control. Supplementary movie S1 shows that the conventional cellulose paper burned completely within 3s after exposure to the flame sourced from the alcohol lamp, which is the drawbacks of conventional commercial cellulose paper to construct flexible conductive materials. To understand the flame retardancy of silver-coated MAFP, the sample with a size of 30 mm in length and 5 mm in width was exposed to flame and the electrical current through the silver-coated MAFP connected with a direct current power supply at 3 V and a bulb was recorded. It was found that the electrical current remained nearly unchanged when the sample was in contact with the flame for 8 s (Fig. 5c). After 8s, the sample started to burn due to the high temperature of alcohol lamp (the temperature of the flame was 600 °C) (Fig. 5e) and this resulted in a slight decrease of the electrical current by 0.05 A. This change can be explained by the oxidation of Ag, forming and decomposition of Ag_2O and the damage of substrate structure. When the silver-coated MAFP was moved from the flame after 15 s, it stopped burning, the electrical current remained at 0.21 A and the light bulb remained lit. The entire process (Supplementary movie S2) proves that the silver-coated MAFP is flame-retardant and can be used as flame-retardant flexible conductive materials.

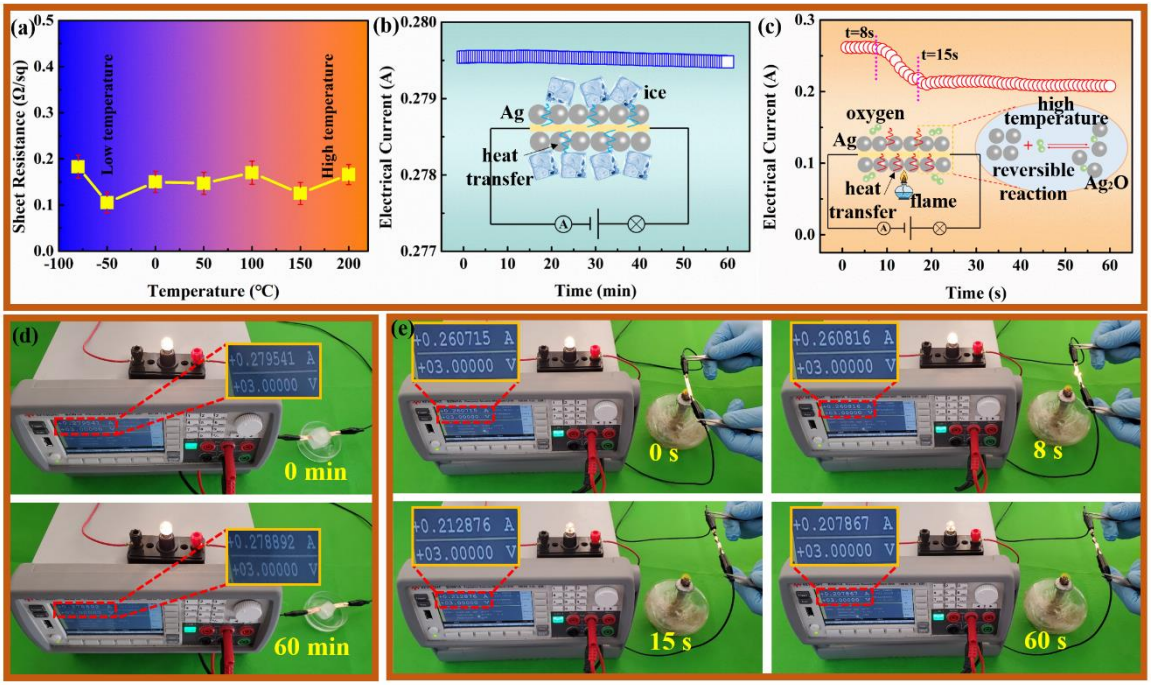

Fig. 5. The variation of sheet resistance for silver-coated MAFP in the temperature range of -80 – 200 °C (a); evaluation of electrical conductivity of silver-coated MAFP in contact with ice (b) and flame (c); electrical current through the silver-coated MAFP connected with a direct current power supply at 3 V and a bulb during the exposure process of the paper to ice (d) and flame (e) at different time.

To further study the reliability of silver-coated MAFP, a variety of verification tests were performed by exposing the sample to acid/alkali solutions and various chemical solvents. Silver-coated MAFP with a size of 20 mm in length and 5 mm in width was immersed in different solutions including hydrochloric acid (pH = 2.0), deionized water (pH = 7.0), sodium hydroxide (pH = 12.0), and various organic solvents including N-heptane, acetone, ethanol, xylene and DMF, the sheet resistance was measured after soaking in the solutions/solvents for different time periods. Fig. 6a shows the variation in sheet resistance

of silver-coated MAFP after soaking in acid/alkali solutions and organic solvents for 7 days. We can see that the sheet resistance increased by 9.7%, 13.0%, 19.1% and 32.2% respectively after soaking in N-heptane, acetone, ethanol and xylene for 7 days, but the highest sheet resistance after immersion in the above solvents was less than 0.3 Ω/sq, indicating good electrical conductivity. It should be noted that the sheet resistance of silver-coated MAFP increased remarkably by 587.0% after soaking in DMF for 7 days. It can be envisaged that this substantial change in electrical conductivity was related to the interaction between DMF and MAFP. DMF, a good solvent of *meta*-aramid [49], can easily cause the destruction of the integrity structure of MAFP substrate which is responsible for the observed increase in electrical resistance. It can also be seen from Fig. 6a that the sheet resistance increased by 19.8%, 2.2% and 17.3% respectively after soaking in an acid solution with pH of 2.0, deionized water with pH of 7.0 and an alkali solution with pH of 12.0. This should be a slight corrosion of the samples induced by acid and alkali, but the sheet resistance after immersion was less than 0.3 Ω/sq. These results have clearly demonstrated that the silver-coated MAFP can maintain excellent conductivity in both acid/alkali solutions and organic solvents, except DMF which can dissolve the MAFP substrate.

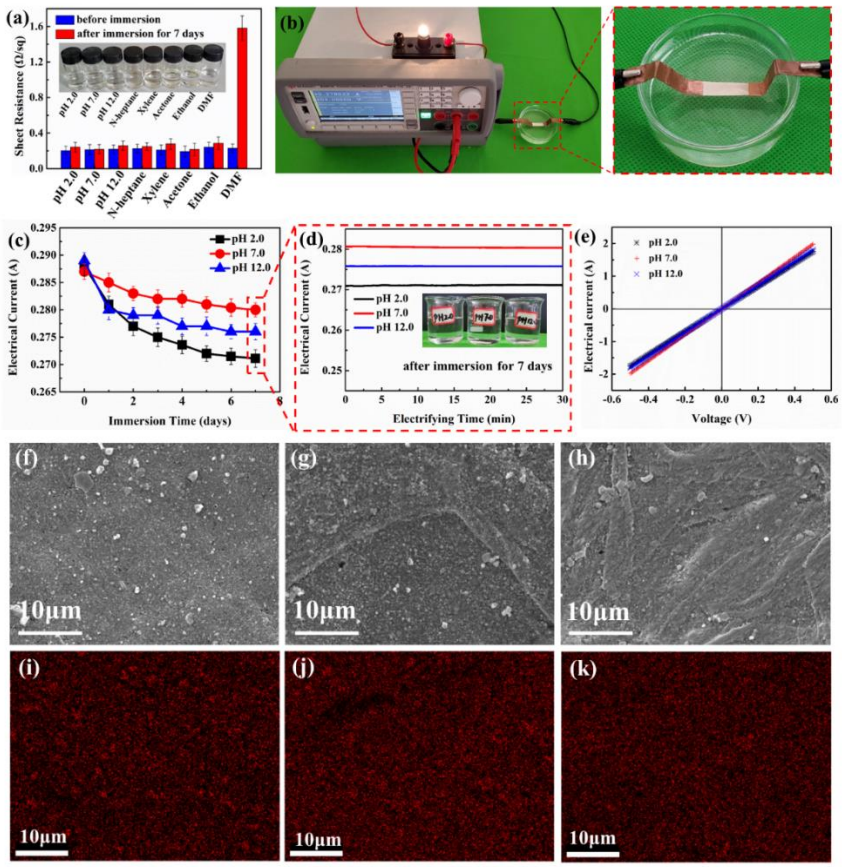

Fig. 6. Comparison of sheet resistance for silver-coated MAFP before and after immersion in acid/alkali solution and organic solvents for 7 days (a); electrochemical corrosion test setup for silver-coated MAFP in acid/neutral/alkali solution (b); the variation of electrical current during the exposure process of silver-coated MAFP to acid/neutral/alkali solution for different time (c); the variation of electrical current with electrifying time for the circuit with silver-coated MAFP immersed in solutions with different pH values for 7 days (d); the volt-ampere characteristic curve of silver-coated MAFP after soaking in solutions with different pH values for 7 days (e); SEM images and EDS mapping of Ag element for silver-coated MAFP after immersion in solutions with pH of 2.0 (f, i), 7.0 (g, j) and 12.0 (h, k) for 7 days.

In order to further evaluate the anti-corrosion property of silver-coated MAFP, electrochemical corrosion in acid/alkali solution was conducted. Silver-coated MAFP which had been immersed in solutions with pH value of 2.0, 7.0 and 12.0 for different times was connected with a power supplier (B2901A, Keysight, USA) and a bulb to form an electric circuit during the exposure process of the paper to the above solutions, as shown in Fig. 6b. The variation in electrical current was recorded for 30 min. The electrical current through the silver-coated MAFP which was exposed to acid/neutral/alkali solution was stable during the electrifying process (Fig. S3, Supplementary data). Moreover, compared to the circuit connected with pristine silver-coated MAFP, the electrical current of the circuit connected with the silver-coated MAFP which had been immersed in the solution with different pH values for 7 days decreased by only 5.87%, 2.5% and 4.5% respectively (Fig. 6c). The electrical current of the circuit with the silver-coated MAFP immersed for 7 days was still highly stable (Fig. 6d). The anti-corrosion property of the silver-coated MAFP is related to the chemical stability of Ag and MAFP substrate, the silver barely reacts with H^+/OH^- according to the order of metal activity and meanwhile benzene ring and amide bond in the *meta*-aramid molecule form a conjugation effect, which hinders its reaction with external ions [50]. The volt-ampere characteristics of the silver-coated MAFP after immersion in solutions with pH of 2.0, 7.0 and 12.0 for 7 days also adhered to the Ohs' law as shown in Fig. 6e. Surface morphology observation and the elemental mapping of Ag element confirmed the integrity of surface coating after immersion (Fig. 6f - k). These results clearly suggest that the prepared silver-coated MAFP has excellent acid/alkali stability and is feasible to be used as anti-corrosive flexible conductive materials.

3.4. Electromagnetic interference shielding performance

Finally, we demonstrated the application of silver-coated MAFP in electromagnetic interference (EMI) shielding. The EMI shielding effectiveness (SE) of pristine MAFP was close to zero (Fig. S4, Supplementary data), indicating that MAFP did not have electromagnetic shielding effectiveness. As shown in Fig. 7a, the silver-coated MAFP had an EMI SE of as high as 95.47 dB. The specific EMI shielding effectiveness (SE divided by the thickness of the material) reached 530.38 $dB \cdot mm^{-1}$, which was higher than previously reported EMI shielding materials (Fig. 7b and Table S1). These favorable results highlight the silver-coated MAFP in high-performance EMI shielding application. The EMI shielding mechanism was analyzed to understand the high EMI shielding performance of the silver-coated MAFP. It is known that the total EMI SE (SE_{Total}) is the sum of the shielding effectiveness of absorption loss (SE_A), reflection loss (SE_R) and multiple reflection (SE_M), where SE_M is generally negligible when the value of SE_{Total} is above 15 dB [51-53]. It can be noted from Fig. 7a that the SE_A (84.56 dB) was always much higher than SE_R (10.91 dB) over the entire frequency range. Although, the SE_A was larger than SE_R, the silver-coated MAFP was not an electromagnetic wave adsorption material. As known, reflection mainly occurs on the material surface while SE absorption refers to the attenuation of electromagnetic waves which filters into the material. The shielding mechanism is determined by the power coefficient of reflectance (R), absorbance (A) and transmittance (T) [54]. The R and A of the silver-coated MAFP was 91.9% and 8.1% respectively, indicating most of the electromagnetic waves were reflected rather than absorbed. Therefore, the reflection mechanism played a dominant role in attenuating the electromagnetic waves for the silver-coated MAFP. Skin depth (δ) which is defined as the depth at which the amplitude of electromagnetic wave decreases exponentially to 1/e of its original value, is an important

physical parameter for the shielding ability. The δ value of the silver-coated MAFP can be calculated by using the Eqn. (2) [55].

$$\delta = \sqrt{\frac{1}{\pi f \mu \sigma}} \quad \text{when } \sigma >> 2\pi f \varepsilon_0,\ \mu = \mu_0 \mu_r \qquad (2)$$

The achieved δ value at 8.2 GHz and 12.4 GHz for the silver-coated MAFP was 0.029 mm and 0.024 mm respectively, which is much thinner than the thickness of the tested sample of 0.18 mm. The theoretical SE_{total}, SE_R, and SE_A were carried out based on the well-materialized reports (detailed calculations were shown in Supplementary data). The theoretical SE_{total}, SE_R, and SE_A was 100.3 dB, 35.23 dB and 65.1 dB respectively. The theoretical SE_{total} was in good agreement with experimental value. In comparison to theoretical results, the experimental results showed a slight lower *R* and a higher *A*. This is because there were massive interface areas between the *meta*-aramid fibers and the conductive silver nanoparticles in the silver-coated MAFP, which were available for repeatedly reflection and scattering to prolong the microwave transmission routes. As a consequence, electromagnetic waves were difficult to escape before being absorbed and dissipated as heat [56].

Fig. 7c shows the EMI SE of silver-coated MAFP after 5 washing cycles, 1000 bending cycles and soaking in acid/alkali solutions and various organic solvents for 7 days. It can be seen that the electromagnetic shielding effectiveness of silver-coated MAFP after washing, bending and soaking in solutions of acid solution (pH = 2.0), alkali solution (pH = 12.0), ethanol, acetone, N-heptane and xylene was 59.08 dB, 64.57 dB, 61.67 dB, 88.64 dB, 73.06 dB, 71.41 dB, 81.34 dB and 81.19 dB, respectively, which far exceeds the commercial requirement of 30 dB for EMI shielding materials [12]. The excellent stability of EMI SE

originates from the stable electrical conductivity of the silver-coated MAFP after being immersed in acid/alkali solution and various organic solvents as demonstrated in Fig. 6a.

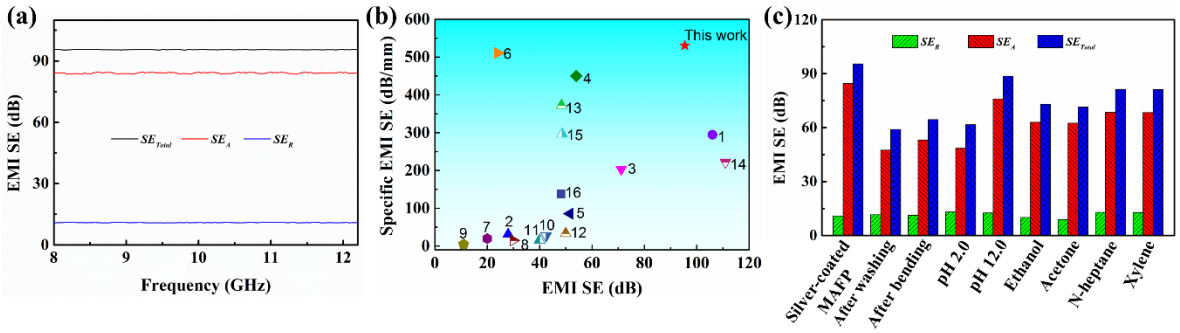

Fig. 7. The SE_{Total}, SE_A and SE_R of silver-coated MAFP (a); comparison of EMI SE for silver-coated MAFP and the previously reported shielding materials (the corresponding references are given in Table S1) (b) and the EMI SE of silver-coated MAFP after 5 washing cycles, 1000 bending cycles and soaking in acid/alkali solutions and various solvents soaking for 7 days (c).

4. Conclusions

In conclusion, we have fabricated flexible and electrically conductive MAFP paper with excellent thermal and chemical stability by combining low-temperature oxygen plasma treatment and electroless silver plating. The plasma treatment played a critical role in facilitating the effective deposition of silver nanoparticles on the MAFP surface and improving the coating durability through the introduction of active oxygen-containing groups. The silver-coated MAFP had an electrical resistance as low as 0.152 Ω/sq and reliable washing/bending fastness, high/low temperature stability and chemical resistance. The high electrical conductivity contributed the silver-coated MAFP an excellent EMI shielding performance with an EMI SE of 95.47 dB and a specific SE of 530.38 $dB \cdot mm^{-1}$. Therefore,

we expect that the electrically conductive MAFP paper is promising for applications in various flexible EMI shielding devices with the ability of working under extreme conditions.

Acknowledgements

The authors would like to thank the financial support from the Shandong Provincial Key Research and Development Program, China (Grant no. 2019GGX102071, 2018GGX108003), the National Key Research and Development Program of China (Grant no. 2017YFB0309805-2), the Shandong "Taishan Youth Scholar Program", the National Natural Science Foundation of China (Grant no. 51703108) and the Shandong Provincial Natural Science Foundation, China (Grant no. ZR2017BEM042).

Appendix A. Supplementary data

The cross section morphology of silver-coated MAFP; SEM image of silver-coated MAFP without plasma treatment; the electrical resistance of silver-coated MAFP with and without plasma treatment; electrochemical corrosion test data; the calculation of EMI SE and the EMI SE of pristine MAFP.

Movie S1 showing the burning process of conventional cellulose paper.

Movie S2 showing the burning process of silver-coated MAFP with plasma treatment.

References

[1] H. Wu, Y. Huang, F. Xu, Y. Duan, Z. Yin, Energy harvesters for wearable and stretchable electronics: from flexibility to stretchability, Adv. Mater. 28 (2016) 9881-9919.
[2] Y. Yang, Q. Huang, L. Niu, D. Wang, C. Yan, Y. She, Z. Zheng, Waterproof, ultrahigh areal-capacitance, wearable supercapacitor fabrics, Adv. Mater. 29 (2017) 1606679.
[3] C.B. Liang, K.P. Ruan, Y.L. Zhang, J.W. Gu, Multifunctional flexible electromagnetic interference shielding silver nanowires/cellulose films with excellent thermal management and Joule heating performances, ACS Appl. Mater. Inter. 12 (2020) 18023-18031.
[4] W. Xiong, H. Liu, Y. Chen, M. Zheng, Y. Zhao, X. Kong, Y. Wang, X. Zhang, X. Kong, P. Wang, L. Jiang, Highly conductive, air-stable silver nanowire@iongel composite films toward flexible transparent electrodesm, Adv. Mater. 28 (2016) 7167-7172.

[5] L. Han, K.Z. Liu, M.H. Wang, K.F. Wang, L.M. Fang, H.T. Chen, J. Zhou, X. Lu, Mussel-Inspired Adhesive and Conductive Hydrogel with Long-Lasting Moisture and Extreme Temperature Tolerance, Adv. Funct. Mater. 28 (2018) 1704195.
[6] L. Dong, C. Hu, L. Song, X. Huang, N. Chen, L. Qu, A large-area, flexible, and flame-retardant graphene paper, Adv. Funct. Mater. 26 (2016) 1470-1476.
[7] X. Li, C. Tang, J.N. Wang, W.X. Tian, D. Hu, Analysis and mechanism of adsorption of naphthenic mineral oil, water, formic acid, carbon dioxide, and methane on meta-aramid insulation paper, J. Mater. Sci. 54 (2019) 8556-8570.
[8] F. Yin, C. Tang, X. Li, X.B. Wang, Effect of moisture on mechanical properties and thermal stability of meta-aramid fiber used in insulating paper, Polymers 9 (2017) 537.
[9] J.H. Cai, J. Li, X.D. Chen, M. Wang. Multifunctional polydimethylsiloxane foam with multi-walled carbon nanotube and thermo-expandable microsphere for temperature sensing, microwave shielding and piezoresistive sensor. Chem. Eng. J. 393 (2020)124805.
[10] Y.J. Tan, J. Li, J.H. Cai, X.H. Tang, J.H. Liu, Z.Q. Hu, M. Wang, Comparative study on solid and hollow glass microspheres for enhanced electromagnetic interference shielding in polydimethylsiloxane/multi-walled carbon nanotube composites, Compos. Part B-Eng. 177 (2019) 107378.
[11] J. C. Luo, L. Wang, X.W. Huang, B. Li, Z. Guo, X. Song, L.W. Lin, L.C. Tang, H. G. Xue, J.F. Gao, Mechanically Durable, Highly Conductive, and Anticorrosive Composite Fabrics with Excellent Self-Cleaning Performance for High-Efficiency Electromagnetic Interference Shielding, ACS Appl. Mater. Inter. 11 (2019) 10883-10894.
[12] Y.J. Tan, J. Li, Y. Gao, J. Li, S.Y. Guo, M. Wang, A facile approach to fabricating silver-coated cotton fiber non-woven fabrics for ultrahigh electromagnetic interference shielding, Appl. Surf. Sci. 458 (2018) 236-244.
[13] D.G. Papageorgiou, Z. Li , M. Liu, I.A. Kinloch, R.J. Young, Mechanisms of mechanical reinforcement by graphene and carbon nanotubes in polymer nanocomposites. Nanoscale, 12(2020) 2228-2267.
[14] J.H. Cai, Y.F. Chen, J. Li, Y.J. Tan, J.H. Liu, X.H. Tang, X.D. Chen, M. Wang, Asymmetric deformation in poly(ethylene-co-1-octene)/multi-walled carbon nanotube composites with glass micro-beads for highly piezoresistive sensitivity, Chem. Eng. J. 370 (2019), 176-184.
[15] Y. Wang, W. Li, Y. Zhou, L. Jiang, J. Ma, S. Chen, S. Jerrams, F. Zhou, Fabrication of high-performance wearable strain sensors by using CNTs-coated electrospun polyurethane nanofibers, J. Mater. Sci., 55 (2020) 12592-12606.
[16] Y.F. Chen, J. Li, J.H. Cai, Y.J Tan, X.H. Tang, J.H. Liu, M. Wang, Negative liquid sensing effect and tunable piezoresistive sensitivity in polydimethylsiloxane/carbon nanotubes/water-absorbing-expansion particles nanocomposites, Compos. Part A-Appl. S. 126 (2019), 105608.
[17] J. Bustillos, C. Zhang, B. Boesl, A. Agarwal, Three-dimensional graphene foam-polymer composite with superior deicing efficiency and strength, ACS Appl. Mater. Inter. 10 (2018) 5022-5029.
[18] W. Li, Y.F. Zhou, Y.H. Wang, Y. Li, L. Jiang, J.W. Ma, S.J. Chen, Highly Stretchable and Sensitive SBS/Graphene Composite Fiber for Strain Sensors. Macromol. Mater. Eng. 305 (2020) 1900736.

[19] X.T. Yang, S.G. Fan, Y. Li, Y.Q. Guo, K.P. Ruan, Y.G. Li, K.P. Ruan, S.M. Zhang, J.L. Zhang, J. Kong, J.W. Gu, Synchronously improved electromagnetic interference shielding and thermal conductivity for epoxy nanocomposites by constructing 3D copper nanowires/thermally annealed graphene aerogel framework, Compos. Part A-Appl. S. 128 (2020) 105670.
[20] Y.F. Zhou, L. Jiang, Y. Guo, Z.H. Sun, Z.Q. Jiang, S.J. Chen, J.M. Ma, S. Jerrams, Rapid fabrication of silver nanoparticle/polydopamine functionalized polyester fibers, Tex. Res. J. 89 (2019) 3968-3978.
[21] C.M. Liu, J. Liu, X. Ning, S.J. Chen, Z.Q. Liu, S.X. Jiang, D.G. Miao, The effect of polydopamine on an Ag-coated polypropylene nonwoven fabric, Polymers 11 (2019) 627.
[22] T.T. Li, Y.T. Wang, H.K. Peng, X.F. Zhang, B.C. Shiu, J.H. Lin, C.W. Lou, Lightweight, flexible and superhydrophobic composite nanofiber films inspired by nacre for highly electromagnetic interference shielding, Compos. Part A-Appl. S. 128 (2020) 105685.
[23] G.C. He, X.Z. Dong, J. Liu, H. Lu, Z.S. Zhao, Investigate the electrical and thermal properties of the low temperature resistant silver nanowire fabricated by two-beam laser technique, Appl. Surf. Sci. 439 (2018) 96-100.
[24] B. Vasconcelos, K. Vediappan, J.C. Oliveira, C. Fonseca, Mechanically robust silver coatings prepared by electroless plating on thermoplastic polyurethane, Appl. Surf. Sci. 443 (2018) 39-47.
[25] Y. Mao, M.F. Zhu, W. Wang, D. Yu, Well-defined silver conductive pattern fabricated on polyester fabric by screen printing a dopamine surface modifier followed by electroless plating, Soft Matter 14 (2018) 1260-1269.
[26] C. Gritti, S. Raza, S. Kadkhodazadeh, B. Kardynal, R. Malureanu, N.A. Mortensen, A.V. Lavrinenko, Broadband infrared absorption enhancement by electroless-deposited silver nanoparticles, Nanophotonics 6 (2017) 289-297.
[27] M. Montazer, A. Shamei, F. Alimohammadi, Synthesis of nanosilver on polyamide fabric using silver/ammonia complex, Mater. Sci. Eng. C-Mater. 38 (2014) 170-176.
[28] W.C. Wang, R.Y. Li, M. Tian, L. Liu, H. Zou, X.Y. Zhao, L.Q. Zhang, Surface silverized meta-aramid fibers prepared by bio-inspired poly(dopamine) functionalization, ACS Appl. Mater. Inter. 5 (2013) 2062-2069.
[29] J.J. Chen, Q. An, R.D. Rodriguez, E. Sheremet, Y. Wang, E. Sowade, R.R. Baumann, Z.S. Feng, Surface modification with special morphology for the metallization of polyimide film, Appl. Surf. Sci. 487 (2019) 503-509.
[30] D.L. Chai, Z.M. Xie, Y.S. Wang, L. Liu, Y.J. Yum, Molecular dynamics investigation of the adhesion mechanism acting between dopamine and the surface of dopamine-processed aramid fibers, ACS Appl. Mater. Inter. 6 (2014) 17974-17984.
[31] L.X. Zhao, W.Z. Liu, M. Xu, Y. Huang, Q.T. Zheng, S.J. Sun, Y.Q. Wang, Study on atmospheric air glow discharge plasma generation based on multiple potentials and aramid fabric surface modification, Plasma Processes Polym. 2019 e1900114.
[32] M. Su, A.J. Gu, G.Z. Liang, L. Yuan, The effect of oxygen-plasma treatment on Kevlar fibers and the properties of Kevlar fibers/bismaleimide composites, Appl. Surf. Sci. 257 (2011) 3158-3167.
[33] A. Pakdel, Y. Bando, D. Golberg, Plasma-assisted interface engineering of boron nitride nanostructure films, ACS Nano 8 (2014) 10631-10639.

[34] W.O. Gordon, G.W. Peterson, E.M. Durke, Reduced chemical warfare agent sorption in polyurethane-painted surfaces via plasma-enhanced chemical vapor deposition of perfluoroalkanes, ACS Appl. Mater. Inter. 7 (2015) 6402-6405.
[35] B. Gehl, A. Fromsdorf, V. Aleksandrovic, T. Schmidt, A. Pretorius, J.I. Flege, S. Bernstorff, A. Rosenauer, J. Falta, H. Weller, M. Baeumer, Structure and chemical effects of plasma treatment on close-packed colloidal nanoparticle layers, Adv. Funct. Mater. 18 (2008) 2398-2410.
[36] C. Aleman, G. Fabregat, E. Armelin, J.J. Buendia, J. Llorca, Plasma surface modification of polymers for sensor applications, J. Mater. Chem. B 6 (2018) 6515-6533.
[37] S. Dou, L. Tao, R.L. Wang, S.E. Hankari, R. Chen, S.Y. Wang, Plasma-assisted synthesis and surface modification of electrode materials for renewable energy, Adv. Mater. 30 (2018) 1705850.
[38] S.D. Wavhal, R.E. Fisher, Hydrophilic modification of polyethersulfone membranes by low temperature plasma-induced graft polymerization, J. Membrane Sci. 209 (2002) 255-269.
[39] E.C. Rangel, G.Z. Gadioli, N.C. Cruz, Investigations on the stability of plasma modified silicone surface, Plasmas and Polymers 9 (2004) 35-48.
[40] A. Zille, M.M. Fernandes, A. Francesko, T. Tzanov, M. Fernandes, F.R. Oliveira, L. Almeida, T. Amorim, N. Carneiro, M.F. Esteves, A.P. Souto, Size and aging effects on antimicrobial efficiency of silver nanoparticles coated on polyamide fabrics activated by atmospheric DBD plasma, ACS Appl. Mater. Inter. 7 (2015) 13731-13744.
[41] Z.L. Ma, S.L. Kang, J.Z. Ma, L. Shao, A.J. Wei, C.B. Liang, J.W. Gu, B. Yang, D.D. Dong, L.F. Wei, Z.Y. Ji, High-performance and rapid-response electrical heaters based on ultraflexible, heat-resistant, and mechanically strong aramid nanofiber/Ag nanowire nanocomposite papers, ACS Nano 13 (2019) 7578-7590.
[42] Y. Yang, Q.B. Huang, G.F. Payne, R.C. Sun, X.H. Wang, A highly conductive, pliable and foldable Cu/cellulose paper electrode enable by controlled deposition of copper nanoparticles, Nanoscale 11 (2019) 725-732.
[43] J.G. Lee, J.H. Lee, S. An, D.Y. Kim, T.G. Kim, S.S. Al-Deyab, A.L. Yarin, S.S. Yoon, Highly flexible, stretchable, wearable, patternable and transparent heaters on complex 3D surfaces formed supersonically sprayed silver nanowires, J. Mater. Chem. A 5 (2017) 6677-6685.
[44] W. Lan, Y. Chen, Z. Yang, W. Han, J. Zhou, Y. Zhang, J. Wang, G. Tang, Y. Wei, W. Dou, Q. Su, E. Xie, Ultraflexible transparent film heater made of Ag nanowire/PVA composite for rapid-response thermotherapy pads, ACS Appl. Mater. Inter. 9 (2017) 6644-6651.
[45] C.X. Wu, T.W. Kima, S. Sung, J.H. Park, F.S. Li, Ultrasoft and cuttable paper-based triboelectric nanogenerators for mechanical energy harvesting, Nano Energy 44 (2018) 279-287.
[46] B. Yao, L.Y. Yuan, X. Xiao, J. Zhang, Y.Y. Qi, J. Zhou, J. Zhou, B. Hu, W. Chen, Paper-based solid-state supercapacitors with pencil-drawing graphite/polyaniline networks hybrid electrodes, Nano Energy 2 (2013) 1071-1078.
[47] S. Choi, J. Park, W. Hyun, J. Kim, Y.B. Lee, C. Song, H.J. Hwang, J.H. Kim, T. Hyeon, D.H. Kim, Stretchable heater using ligand-exchanged silver nanowire nanocomposite for wearable articular thermotherapy, ACS Nano 9 (2015) 6626-6633.

[48] F.F. Chen, Y.J. Zhu, Z.C. Xiong, L.Y. Dong, F. Chen, B.Q. Lu, R.L. Yang, Hydroxyapatite nanowire-based all-weather flexible electrically conductive paper with superhydrophobic and flame-retardant properties, ACS Appl. Mater. Inter. 9 (2017) 39534-39548.
[49] J. Chung, S.Y. Kwak, Solvent-assisted heat treatment for enhanced chemical stability and mechanical strength of meta-aramid nanofibers, Eur. Polym. J. 107 (2018) 46-53.
[50] J. Zhu, M. Yang, A. Emre, J.H. Bahng, L.Z. Xu, J. Yeom, B. Yeom, Y. Kim, K. Johnson, P. Green, N. Kotov, Branched aramid nanofibers, Angew. Chem. Int. Edit. 56 (2017) 11744-11748.
[51] Z.R. Jia, K.C. Kou, S. Yin, A.L. Feng, C.H. Zhang, X.H. Liu, H.J. Cao, G.L. Wu, Magnetic Fe Nanoparticle to Decorate N Dotted C as An Exceptionally Absorption-dominate Electromagnetic Shielding Material, Compos. Part B-Eng. 189(2020) 107895.
[52] Z. Chen, C. Xu, C. Ma, W. Ren, H.M. Cheng, Lightweight and Flexible Graphene Foam Composites for High-Performance Electromagnetic Interference Shielding. Advanced Materials. 25 (2013) 1296-300.
[53] Z.R. Jia, C. Wang, A.L. Feng, P.B. Shi, C.H. Zhang, X.H. Liu, K.K. Wang, G.L. Wu, A low dielectric decoration strategy to achieve absorption dominated electromagnetic shielding material, Compos. Part B-Eng. 183(2020) 107690.
[54] J.F. Gao, J.C. Luo, L. Wang, X.W. Huang, H. Wang, X. Song, M.J. Hu, L.C. Tang, H.G. Xue, Flexible, superhydrophobic and highly conductive composite based on non-woven polypropylene fabric for electromagnetic interference shielding, Chem. Eng. J. 364 (2019) 493-502.
[55] J. Li, J.L. Chen, X.H. Tang, J.H. Cai, J.H. Liu, M. Wang, Constructing nanopores in poly(oxymethylene)/multi-wall carbon nanotube nanocomposites via poly(l-lactide) assisting for improving electromagnetic interference shielding, J. Colloid. Interf. Sci. 565 (2020) 536-545.
[56] L.C. Jia, L. Xu, F. Ren, P.G. Ren, D.X. Yan, Z.M. Li, Stretchable and durable conductive fabric for ultrahigh performance electromagnetic interference shielding, Carbon 144 (2019) 101-108.